Published in final edited form as:
J Magn Reson. 2007 May ; 186(1): 51–64. doi:10.1016/j.jmr.2007.01.014.

Triple resonance experiments for aligned sample solid-state NMR of ^{13}C and ^{15}N labeled proteins

Neeraj Sinha[a], **Christopher V. Grant**[a], **Sang Ho Park**[a], **Jonathan Miles Brown**[b], and **Stanley J. Opella**[a,*]

[a]Department of Chemistry and Biochemistry, University of California, San Diego, 9500 Gilman Drive, 0307 La Jolla, CA 92093-0307, USA

[b]ProSpect Pharma, Inc., 9108A Guilford Road, Columbia, MD 21046, USA

Abstract

Initial steps in the development of a suite of triple-resonance $^{1}H/^{13}C/^{15}N$ solid-state NMR experiments applicable to aligned samples of ^{13}C and ^{15}N labeled proteins are described. The experiments take advantage of the opportunities for ^{13}C detection without the need for homonuclear $^{13}C/^{13}C$ decoupling presented by samples with two different patterns of isotopic labeling. In one type of sample, the proteins are ~20% randomly labeled with ^{13}C in all backbone and side chain carbon sites and ~100% uniformly ^{15}N labeled in all nitrogen sites; in the second type of sample, the peptides and proteins are ^{13}C labeled at only the α-carbon and ^{15}N labeled at the amide nitrogen of a few residues. The requirement for homonuclear $^{13}C/^{13}C$ decoupling while detecting ^{13}C signals is avoided in the first case because of the low probability of any two ^{13}C nuclei being bonded to each other; in the second case, the labeled $^{13}C_{\alpha}$ sites are separated by at least three bonds in the polypeptide chain. The experiments enable the measurement of the ^{13}C chemical shift and $^{1}H–^{13}C$ and $^{15}N–^{13}C$ heteronuclear dipolar coupling frequencies associated with the $^{13}C\alpha$ and $^{13}C'$ backbone sites, which provide orientation constraints complementary to those derived from the ^{15}N labeled amide backbone sites. $^{13}C/^{13}C$ spin-exchange experiments identify proximate carbon sites. The ability to measure $^{13}C–^{15}N$ dipolar coupling frequencies and correlate ^{13}C and ^{15}N resonances provides a mechanism for making backbone resonance assignments. Three-dimensional combinations of these experiments ensure that the resolution, assignment, and measurement of orientationally dependent frequencies can be extended to larger proteins. Moreover, measurements of the ^{13}C chemical shift and $^{1}H–^{13}C$ heteronuclear dipolar coupling frequencies for nearly all side chain sites enable the complete three-dimensional structures of proteins to be determined with this approach.

Keywords

PISEMA; HETCOR; Isotopic labeling; Dipolar coupling; Oriented proteins

1. Introduction

The vast majority of applications of aligned-sample solid-state NMR spectroscopy to proteins have utilized $^{1}H/^{15}N$ double resonance experiments [1–3]. This reflects the relative ease of ^{15}N labeling of proteins by expression in bacteria, the strategic locations of the amide nitrogens within the planes of the polypeptide backbone, and the favorable

*Corresponding author. Fax: +1 858 822 4821. sopella@ucsd.edu (S.J. Opella).

spectroscopic properties of the directly bonded pair of ^{1}H and ^{15}N nuclei in each amide site [4]. Even when all nitrogen sites in a protein are labeled with ^{15}N, these nuclei behave as if they are “dilute” because of the combination of their low gyromagnetic ratio and spatial isolation. Three bonds separate the backbone amide nitrogens, and there are no directly bonded pairs of nitrogen atoms in polypeptides. Consequently, it is unnecessary to incorporate homonuclear $^{15}N/^{15}N$ decoupling at any stage of the SLF (separated local field) [5] and HETCOR (heteronuclear correlation) experiments that yield well resolved two- and three-dimensional spectra of proteins, and are used to measure the orientationally dependent ^{1}H chemical shift, $^{1}H–^{15}N$ heteronuclear dipolar coupling, and ^{15}N chemical shift frequencies that are input for the structure calculations. However, it is desirable to measure frequencies from additional spin interactions, especially those associated with carbon atoms, in order to include the side chains in the structure determinations, and to improve the precision and accuracy of the structure calculations.

$^{1}H/^{13}C/^{15}N$ triple-resonance experiments are widely employed in both solution-state NMR [6] and MAS (magic angle spinning) solid-state NMR of proteins [7,8]. Initial steps in the development of a suite of triple-resonance solid-state NMR experiments applicable to aligned samples of ^{13}C and ^{15}N labeled proteins are described in this article. These experiments enable the measurement of the ^{13}C chemical shift and $^{1}H–^{13}C$ and $^{15}N–^{13}C$ heteronuclear dipolar coupling frequencies associated with the $^{13}C_{\alpha}$ and $^{13}C'$ backbone sites. These frequencies provide orientation constraints complementary to those derived from the ^{15}N labeled amide backbone sites, and will improve the quality of structure determinations. In particular, with a sufficient number of heteronuclear dipolar couplings measurements, there is the possibility of improving the precision of the calculated protein structure calculations by avoiding the use of the chemical shift frequencies that are the largest source of uncertainty due to residue-to-residue variations of the chemical shift tensors. Moreover, measurements of the ^{13}C chemical shift and $^{1}H–^{13}C$ heteronuclear dipolar coupling frequencies for nearly all side chain sites will enable the complete three-dimensional structures of proteins to be determined with this approach.

Despite these well-established benefits, only a few triple-resonance experimental results relevant to aligned-sample solid-state NMR have been reported. This is largely because of the difficulty in implementing C detection on uniformly ^{13}C labeled molecules with their dense network of homonuclear $^{13}C/^{13}C$ couplings among the directly bonded carbons. The triple-resonance solid-state NMR experiments described in this article take advantage of the opportunities for ^{13}C detection without the need for homonuclear $^{13}C/^{13}C$ decoupling presented by samples with two different patterns of isotopic labeling. In one type of sample, the proteins are ~20% randomly labeled with ^{13}C in all backbone and side chain carbon sites and ~100% uniformly ^{15}N labeled in all nitrogen sites. Similar labeling schemes have been used in solution NMR studies of biomolecules [9,10]. In the second type of sample, the peptides and proteins are ^{13}C labeled at only the α-car-bon and ^{15}N labeled at the amide nitrogen of a few residues. The corresponding experiments for the complementary labeling scheme at only the C' sites can be readily envisaged. The requirement for homonuclear $^{13}C/^{13}C$ decoupling while detecting ^{13}C signals is avoided in the first case because of the low probability (~4%) of any two ^{13}C nuclei being bonded to each other. In the second case, the labeled $^{13}C_{\alpha}$ sites are separated by at least three bonds in the polypeptide chain, so in the “worst case”, where two adjacent residues in an α-helix are labeled, the C_{α} sites are separated by 3.8 Å, which results in a maximum $^{13}C/^{13}C$ homonuclear dipolar coupling of 135 Hz when the inter-nuclear vector is parallel to the direction of the magnetic field. This corresponds to about 0.5 ppm in a 21T magnet, and will generally not contribute to the linewidths of the observed resonances; in magnetically aligned bilayer samples (perpendicular bicelles), the corresponding values are 54 Hz and 0.2 ppm, substantially less than the typical 1–2 ppm linewidths of the protein resonances [11].

Complementary approaches that result in alternate sites labeled with ^{13}C have been used in MAS solid-state NMR experiments [7,12], and may also prove useful in aligned sample solid-state NMR with experiments similar to those described here.

We have previously described applications of both ^{15}N- and ^{13}C-detected versions of triple-resonance experiments to single-crystal samples of model peptides, and aligned samples of filamentous bacteriophage particles and membrane proteins in phospholipid bilayers [11,13–17]. Recently, we have reviewed [18] these results and extended them somewhat by constructing a new generation of triple-resonance probes and implementing SPINAL-16 decoupling [19] for greater bandwidth [20]. However, these experiments are fundamentally limited in scope: in order to observe ^{13}C chemical shift frequencies in the spectra, it is necessary to apply homonuclear $^{13}C/^{13}C$ decoupling in an indirect dimension, and utilize ^{15}N detection in the presence of heteronuclear ^{1}H and ^{13}C decoupling at the cost of the sensitivity advantage of ^{13}C detection. An interesting approach to ^{13}C detection of uniformly ^{13}C and ^{15}N labeled samples using band-selective homonuclear decoupling has been described by Ishii and Tycko [21]; however, this does not allow the entire ^{13}C NMR spectrum to be observed in a single experiment. Thus, there is a need for the development of additional triple-resonances experiments applicable to aligned sample solid-state NMR of ^{13}C and ^{15}N labeled proteins [22], especially those that utilize ^{13}C detection for higher sensitivity.

2. Results

Timing diagrams for several two- and three-dimensional $^{1}H/^{13}C/^{15}N$ triple-resonance solid-state NMR experiments are shown in Fig. 1. Experimental spectra demonstrating applications of these pulse sequences to ^{13}C and ^{15}N labeled peptides and proteins are presented in Figs. 2–13. Four different samples are used for the demonstrations of pulse sequences:

- **i.** $^{13}C_{\alpha}$, ^{15}N labeled single crystal of N-acetyl leucine ($^{13}C_{\alpha}$, ^{15}N NAL);
- **ii.** ^{15}N labeled single crystal of N-acetyl valine (NAV);
- **iii.** Pf1 coat protein in magnetically aligned phospholipid bilayers where the protein is labeled with $^{13}C_{\alpha}$ and ^{15}N at all valine, leucine and isoleucine residues ($^{13}C_{\alpha}$, ^{15}N VLI Pf1);
- **iv.** Pf1 coat protein in magnetically aligned bacteriophage particles where the protein is labeled ~20% randomly with ^{13}C and ~100% uniformly with ^{15}N Pf1 (^{13}C, ^{15}N Pf1).

The one-dimensional spectra in Fig. 2 demonstrate the improvement (approximately fourfold) in signal to noise ratio that results from ^{13}C detection compared to ^{15}N detection with as many other factors as possible kept constant. The spectra in Fig. 2a – c were obtained from the single crystal sample of $^{13}C_{\alpha}$ and ^{15}N labeled *N*-acetyl-leucine ($^{13}C_{\alpha}$, ^{15}N NAL). The four lines in the spectra reflect the four unique molecular orientations in the unit cell of the crystal. The fully decoupled one-dimensional ^{13}C Fig. 2a) and ^{15}N (Fig. 2b) NMR spectra were obtained by conventional single-contact spin-lock cross-polarization [23]. The ^{13}C NMR spectrum in Fig. 2c was obtained by double-cross-polarization [24] with transfers of magnetization from ^{1}H to ^{15}N to ^{13}C in successive steps. The double-cross-polarization procedure is not as effective as direct cross-polarization in generating ^{13}C magnetization, nonetheless, the signal to noise ratio of the spectrum in Fig. 2c is substantially higher than that observed with simple ^{15}N cross-polarization and detection (Fig. 2b). The ^{13}C resonance at 62 ppm in the double-cross-polarization spectrum in Fig. 2c has noticeably lower intensity than the other resonances because its very

small ^{13}C–^{15}N dipolar coupling (as observed with other experiments, e.g. Fig. 8a) reduces the relative efficiency of the ^{15}N to ^{13}C transfer step. To a lesser extent, this is the case for the ^{13}C resonance at 35 ppm, since it too has reduced intensity in experiments with transfers that rely on ^{13}C–^{15}N dipolar couplings. The extent of magnetization transfer between ^{15}N and ^{13}C depends mainly upon the magnitude of the ^{13}C–^{15}N dipolar coupling and the length of the mix time for cross-polarization. The experiments were individually optimized for maximum signal intensity by varying the mix time for the transfer; for relatively weak ^{13}C–^{15}N couplings (<200 Hz), maximum transfer occurs with a 5.0 ms mix time; in contrast, for larger C- N couplings (~1 kHz) a mix time of 1.0 ms yields the largest signals. The comparison of the N- (Fig. 2d) and ^{13}C- (Fig. 2e) detected cross-polarization spectra demonstrates similar improvements for a double-labeled membrane protein in magnetically aligned bilayers. In this example, the 46-residue coat protein of the filamentous bacteriophage Pf1 is selectively labeled in the valine, leucine, and isoleucine residues with $^{13}C_\alpha$ and ^{15}N ($^{13}C_\alpha$, ^{15}N VLI Pf1). Although a portion of the signal intensity in Fig. 2e comes from the natural abundance ^{13}C background from the lipids and the protein, most of the increase in the amplitude relative to that in Fig. 2d is due to signals from the labeled residues.

2.1. PISEMA

The pulse sequence for two-dimensional PISEMA (polarization inversion spin exchange at the magic angle) applicable to ^{13}C and ^{15}N labeled samples shown in Fig. 1a is compatible with either ^{13}C or ^{15}N detection. This triple-resonance version of PISEMA differs from the standard double-resonance experiment [25] in that low power irradiation is applied to the unobserved nucleus during the heteronuclear spin-exchange interval (t_1), and high power irradiation is applied to both ^1H and the unobserved nucleus during data acquisition (t_2). It is intended for situations where homonuclear decoupling of the observed nuclei is unnecessary because of the isotopic or spatial isolation of the labeled sites. In the experiments diagrammed in Fig. 1, the irradiations responsible for heteronuclear decoupling are modulated by SPINAL-16 [19] to increase their bandwidth for high field applications [20] with the exception of the low level continuous wave irradiations applied to the unobserved nuclei in PISEMA-based pulse sequences.

The two-dimensional ^1H–^{13}C PISEMA spectra in Fig. 3 demonstrate that all ^{13}C sites in peptides, including those without directly bonded hydrogens, e.g. carbonyl and carboxyl carbons, have measurable ^1H–^{13}C heteronuclear dipolar couplings. The two-dimensional spectrum in Fig. 3a was obtained on the single crystal sample of $^{13}C_\alpha$, ^{15}N NAL and each of the $^{13}C_\alpha$ resonances has a different ^1H–^{13}C dipolar coupling frequency between about 3 and 17 kHz. All of the dipolar coupling frequencies are reported as half the total splitting, since one half of the spectrum is displayed, which is symmetric about the zero frequency. For comparison, the spectrum in Fig. 3b was obtained on a single crystal sample of ^{15}N labeled *N*-acetylvaline (NAV) with all of the carbon sites in natural isotopic abundance. There are eight distinct resonances from the carbonyl and carboxyl carbons (one each in each of four unique molecules in the unit cell) between 95 and 240 ppm in the spectrum in Fig. 3b, and each of them has discernable ^1H–^{13}C heteronuclear dipolar couplings varying between 2 and 4 kHz. The $^{13}C_\alpha$ resonances are recognizable as single peaks between 30 and 55 ppm. Other aliphatic carbons contribute more complex patterns [26] to the spectrum between 10 and 40 ppm. The ^{13}C chemical shift and ^1H–^{13}C dipolar coupling frequencies and spectral patterns demonstrate the potential for using long-range heteronuclear dipolar couplings as distance and angular constraints for the carbonyl and carboxyl carbons as well as for obtaining angular constraints on the aliphatic side chains.

The two-dimensional ^1H–^{13}C PISEMA spectrum of a selectively $^{13}C_\alpha$, ^{15}N labeled membrane protein in magnetically aligned bilayers is shown in Fig. 4. Pf1 coat protein has a

total of fifteen valine, leucine, and isoleucine residues, nine of which are in the transmembrane helix and contribute resonances (within the box) to the spectrum in Fig. 4; their ^{1}H–^{13}C dipolar couplings range between 2.7 and 5.8 kHz with ^{13}C chemical shift frequencies between 54 and 70 ppm. Nearly all of the other signals in the spectrum are from the natural abundance background of the lipids, as verified by comparison with a spectrum of a similar sample without ^{13}C labels in the protein. These data provide access to two orientationally dependent frequencies at the α carbon sites, which are valuable complements to the previously available frequencies associated with the amide nitrogen sites.

The two-dimensional NMR spectrum in Fig. 5 was obtained from the structural form of the Pf1 coat protein in magnetically aligned bacteriophage particles [27]. In this sample, the protein is randomly labeled with ~20% ^{13}C and ~100% uniformly labeled with N. For economy of presentation, the portion of the C NMR spectrum between 80 and 160 ppm that does not contain signal intensity is not shown. The two-dimensional NMR spectrum in Fig. 5 shows that resonances from carbonyl and carboxyl carbons (160–220 ppm), C_α (55–75 ppm) and aliphatic side chain carbons (5–55 ppm) have substantial heteronuclear ^{1}H- C dipolar couplings. The several hundred discernable resonances in this spectrum indicate the potential for analyzing essentially all carbon sites in a protein with this approach.

Two-dimensional ^{1}H–^{15}N PISEMA experiments can be performed with ^{13}C detection using the pulse sequence shown in Fig. 1d. After the t_1 period, during which the spin exchange between ^{1}H and ^{15}N nuclei takes place, the ^{15}N magnetization is transferred to ^{13}C by cross-polarization. The ^{13}C signals modulated by the ^{1}H–^{15}N heteronuclear dipolar couplings are detected during t_2 in the presence of both ^{1}H and ^{15}N heteronuclear decoupling. A short (1.5 ms) ^{15}N to ^{13}C cross-polarization mix time ensures selective one bond polarization transfers. The resulting two-dimensional spectrum correlates ^{1}H–^{15}N dipolar coupling and ^{13}C chemical shift frequencies.

Fig. 6 contains ^{1}H–^{15}N PISEMA spectra of the single crystal sample of $^{13}C_\alpha$, ^{15}N NAL. The spectrum in Fig. 6a was obtained using the pulse sequence in Fig. 1a with ^{15}N detection. The four resonances have ^{1}H–^{15}N dipolar couplings ranging from 300 Hz to 6.0 kHz at this orientation of the crystal. Fig. 6b is a ^{13}C-detected ^{1}H–^{15}N PISEMA spectrum acquired using the pulse sequence shown in Fig. 1d. The double-cross-polarization mix time for the transfer of the magnetization from ^{15}N to ^{13}C was tuned for one bond correlation (1.0 ms). However, the signal at 62 ppm does not yield a dipolar coupling frequency due to the effects of its very small ^{13}C–^{15}N dipolar coupling on cross-polarization efficiency. The signal associated with the ^{13}C resonance at 35 ppm is observable at lower contour levels, consistent with its relatively weak intensity.

2.2. $^{13}C/^{13}C$ homonuclear spin-exchange

A pulse sequence for two-dimensional $^{13}C/^{13}C$ homonuclear spin-exchange [28] spectroscopy is diagrammed in Fig. 1c. Following cross-polarization, the ^{13}C magnetization undergoes chemical shift evolution during t_1 in the presence of both ^{15}N and ^{1}H heteronuclear decoupling; it is then positioned along the z-axis through application of a π/2 pulse with the appropriate phase. After the fixed-length mixing period t_{mix} during which the z component of ^{13}C magnetization evolves in the presence of homonuclear $^{13}C/^{13}C$ dipolar couplings, the ^{13}C magnetization is returned to the transverse plane where it is detected in the presence of H and N hetero-nuclear decoupling.

Fig. 7 contains two-dimensional $^{13}C/^{13}C$ homo-nuclear spin-exchange spectra of the single crystal sample of $^{13}C_\alpha$, ^{15}N NAL. These spectra were obtained at four different mix times (t_{mix}) using the pulse sequence diagrammed in Fig. 1c. The four peaks along the diagonal correspond to the $^{13}C_\alpha$ resonances from the four molecules in the unit cell of the crystal.

The off-diagonal cross-peaks result from homonuclear $^{13}C/^{13}C$ spin exchange between α carbons located on different molecules in the crystal. The internu-clear distances between $^{13}C_\alpha$ sites on different molecules in the crystal vary from 5.7 Å (~40 Hz) to 8.4 A (~13 Hz), and the corresponding splittings are too small to be observed directly in the experimental spectra. For the shorter mix times (1.0–2.0 s) only a limited amount of correlation intensity is observed in the spectra. For the longest mix time (4.5 s), complete correlation among all four molecules in the unit cell can be observed. Since the cross-peaks in these spectra arise from through-space interactions, the experiment strongly discriminates towards proximate pairs of nuclei, and thus provides information about distances between alpha carbons useful for making resonance assignments and as input for structure calculations.

2.3. $^{13}C–^{15}N$ heteronuclear dipolar couplings

The pulse sequence in Fig. 1b can be used to measure $^{13}C–^{15}N$ hetero–nuclear dipolar couplings. The ^{13}C (or ^{15}N) magnetization generated by cross-polarization from ^{1}H evolves during t_1 in the presence of 1H decoupling. The chemical shift evolution that occurs during the t_1 period is refocused and the $^{13}C–^{15}N$ dipolar coupling preserved by the simultaneous application of πpulses in the middle of the period at both the ^{13}C and ^{15}N resonance frequencies. During t_2, the ^{13}C (or ^{15}N) magnetization modulated by the $^{13}C–^{15}N$ coupling is observed in the presence of ^{1}H and ^{15}N (or ^{13}C) heteronuclear decoupling. The resulting two-dimensional spectra have the chemical shift frequencies of the detected (^{13}C or ^{15}N) nuclei along the frequency axis associated with the direct dimension, and the $^{13}C–^{15}N$ heteronuclear dipolar coupling frequencies symmetric about the zero frequency of the indirect dimension. A version of this experiment with multiple π pulse during t_1 on the unobserved nuclei with XY-16 [29] phase cycling is more tolerant of imperfections in the π pulses.

The spectra in Fig. 8 demonstrate the measurement of resolved $^{13}C–^{15}N$ couplings using the pulse sequence in Fig. 1b. The ^{13}C-detected (Fig. 8a) and ^{15}N-detected (Fig. 8b) spectra were obtained on the single crystal sample of $^{13}C_\alpha$, ^{15}N NAL. In both spectra the same $^{13}C–^{15}N$ coupling frequencies are observed, ranging from very small, with no detectable splitting, to 900 Hz. Comparison to the ^{15}N-detected spectrum in Fig. 8b provides a method for cross-assigning ^{13}C and ^{15}N resonances associated with the same residue in a protein.

The data in Fig. 8c were obtained from the single crystal sample of ^{15}N labeled N-acetyl-valine (NAV). The one-dimensional ^{13}C NMR spectrum obtained by cross-polarization is aligned along the ^{13}C chemical shift frequency axis. Four of the carbonyl peaks have vanishingly small $^{13}C–^{15}N$ splitting, as expected for carboxyl carbons, and four have measureable $^{13}C–^{15}N$ splittings between 200 Hz and 1 kHz, as expected for the groups in the peptide linkages. The a carbon signals appear in the range between 40 and 70 ppm, and the other aliphatic carbons give overlapping resonance patterns, as expected, between about 0 and 40 ppm.

As illustrated with the spectra in Fig. 9, it is also possible to observe the $^{13}C–^{15}N$ dipolar couplings in two-dimensional PISEMA spectra through the simple expedient of acquiring the data in the absence of heteronuclear decoupling of the unobserved nucleus. The same four splittings, one of which is very small, along the ^{13}C chemical shift axis (Fig. 9a) and the ^{15}N chemical shift axis (Fig. 9b) are the same. The spectra are more crowded than those in Fig. 8, but clearly provide complementary opportunities for measuring $^{13}C–^{15}N$ dipolar couplings and compiling data that will be useful for making resonance assignments.

2.4. $^{13}C/^{15}N$ HETCOR

The pulse sequence in Fig. 1e correlates the chemical shift frequencies of directly bonded ^{15}N and ^{13}C nuclei, and yields two-dimensional $^{13}C/^{15}N$ HETCOR spectra with ^{13}C and ^{15}N chemical shift frequencies along separate axes. The ^{15}N magnetization generated by cross-polarization from ^{1}H undergoes chemical shift evolution during the incremented t_1 interval in the presence of ^{1}H and ^{13}C heteronuclear decoupling. The ^{15}N magnetization is then transferred to ^{13}C by selective cross-polarization, and the ^{13}C signals are detected in the presence of 1H and ^{15}N heteronuclear decoupling. The phases of the 90° pulses labeled “a” and “b” are chosen to provide phase sensitive quadrature detection in the indirect dimension using the method of States et al. [30].

The presence of both ^{13}C and ^{15}N in the labeled molecules provides opportunities for $^{13}C/^{15}N$ HETCOR experiments. Fig. 10 contains a two-dimensional $^{13}C/^{15}N$ HETCOR spectrum of the single crystal sample of C_α, N NAL. As indicated by the one-dimensional spectra aligned along the ^{13}C chemical shift and ^{15}N chemical shift frequency axes, four resonances are expected. Only three resonances are observed due to the very small $^{13}C–^{15}N$ dipolar coupling at the site with a C chemical shift frequency of 62 ppm. Fig. 11 contains a two-dimensional $^{13}C^{15}N$ HETCOR spectrum of the same ~20% ^{13}C, and ~100% ^{15}N labeled protein sample used to obtain the data in Fig. 5. The $^{13}C/^{15}N$ heteronuclear correlation resonances in Fig. 11a for the carbonyl carbons and in Fig. 11b for the a carbons reflect the proximity of these sites to the ^{15}N labeled amide sites in the peptide linkages in the backbone of the protein. Notably, there are no $^{13}C/^{15}N$ correlation resonances associated with the side chain carbons with ^{13}C chemical shifts between 0 and 40 ppm. This demonstrates the selectivity of the experiments for sites where ^{13}C and ^{15}N are directly bonded.

2.5. Three-dimensional correlation

Three-dimensional experiments will be needed to take full advantage of the possibilities provided by the triple-resonance experiments on proteins with many ^{13}C and ^{15}N labeled sites. The increase in sensitivity that accompanies the use of ^{13}C detection will contribute to the feasibility of routinely applying three-dimensional experiments to aligned protein samples. A three-dimensional triple-resonance correlation experiment is diagrammed in Fig. 1f. The t_1 period of this pulse sequence is the same as that of the PISEMA experiment, and results in the measurement of the $^{1}H–^{13}C$ (or $^{1}H–^{15}N$) dipolar couplings. During the t_2 period, the transverse ^{13}C (or ^{15}N) magnetization evolves under the influence of the heteronuclear $^{13}C–^{15}N$ dipolar coupling, as in the pulse sequence shown in Fig. 1b. Finally, during t_3, ^{13}C (or ^{15}N) magnetization is detected in the presence of two-channel heteronuclear decoupling. The resulting three-dimensional spectra have the ^{13}C chemical shift correlated with $^{1}H–^{13}C$ and $^{13}C–^{15}N$ dipolar couplings. The complementary ^{15}N detected version of the experiment yields three-dimensional spectra where the ^{15}N chemical shifts are correlated with $^{1}H–^{15}N$ and $^{13}C–^{15}N$ dipolar couplings.

Three-dimensional spectra of the single crystal of $^{13}C_\alpha$, ^{15}N NAL are shown in Figs. 12 and 13. The data are presented as three-dimensional cubes, two-dimensional projections, and two-dimensional planes at frequencies corresponding to the four resonances resolved in the chemical shift dimension. Fig. 12 contains results from the ^{13}C detected version of the three-dimensional experiment, and Fig. 13 the ^{15}N-detected version. The cross-sections along the chemical shift planes have $^{1}H–^{13}C$ (or $^{1}H–^{15}N$) and $^{13}C–^{15}N$ dipolar coupling frequency axes. The peaks are labeled in the figures to indicate the cross-assignments between the two experiments. It can be seen that the cross-section of the three-dimensional spectrum correlates two dipolar couplings, $^{1}H–^{13}C/^{13}C–^{15}N$ dipolar coupling in ^{13}C detected versions and $^{1}H–^{15}N/^{13}C–^{15}N$ dipolar couplings in ^{15}N detected versions. Since the cross-sections

from the two versions of the three-dimensional experiments have a common axis of ^{13}C–^{15}N dipolar couplings, this experiment can also complement the chemical shift correlation between ^{13}C and ^{15}N resonance.

3. Discussion

In aligned sample solid-state NMR, the structure and topology of a protein are mapped onto the spectra by the orientation-dependent frequencies resulting from the anisotropic chemical shift and dipole–dipole interactions. Using $^{1}H/^{15}N$ double resonance experiments it has been possible to determine the structures of a number of proteins in virus particles and phospholipid bilayers. However, much more structural information can be gained from the use of ^{13}C and ^{15}N labeled proteins.

The principal advantage of using samples labeled with ^{13}C is the increase in sensitivity associated with the detection of ^{13}C signals. In the peptide and protein examples in Fig. 2, approximately a factor of four increase in signal to noise ratio is observed for ^{13}C detection compared to ^{15}N detection. This can significantly decrease the amount of time required for signal averaging.

The triple-resonance experiments feasible with ^{13}C and ^{15}N labeled samples also provide access to additional orientationally dependent frequencies from the ^{13}C chemical shift and the ^{1}H–^{13}C and ^{13}C–^{15}N heteronuclear dipolar couplings. By themselves, these three frequencies are sufficient to determine the orientation of a peptide plane with respect to the direction of the magnetic field and bilayer normal. Moreover, combinations of ^{1}H–^{15}N, ^{1}H–^{13}C, and ^{13}C–^{15}N dipolar couplings are sufficient to calculate protein structures, and eliminating chemical shift frequencies from the structure calculations has the potential to improve the quality of the resulting structures by eliminating the uncertainties associated with the residue-to-residue variations of the chemical shift tensors.

These experiments provide opportunities for making resonance assignments. $^{13}C/^{13}C$ spin-exchange experiments identify nearby carbon sites by allowing for the broad classification of carbon resonances based on homonuclear $^{13}C/^{13}C$ dipolar coupling strengths. The ability to measure ^{13}C–^{15}N dipolar coupling frequencies and correlate ^{13}C and ^{15}N resonances provides a mechanism for making backbone resonance assignments. Three-dimensional combinations of these experiments ensure that the resolution, assignment, and the measurement of orientationally dependent frequencies can be extended to larger proteins.

These and other opportunities for improvements in resolution, sensitivity, and spectroscopic analysis arising from applications of ^{13}C-detected triple-resonance spectroscopy to aligned protein samples have been reviewed by Vosegaard and Nielsen [22]. Our earlier implementations of triple-resonance spectroscopy were compatible with ^{13}C detection only in a few favorable situations [13–18]. Ishii and Tycko [21] successfully implemented an approach that is generally compatible with uniformly ^{13}C labeled proteins, although it is limited in the range of multi-dimensional experiments it can be applied to by its band-selective characteristics. By combining isotopic labeling schemes with the pulse sequences, we demonstrate the feasibility of triple-resonance spectroscopic experiments capable of simultaneous interrogation of all sites in a protein.

In summary, triple-resonance solid-state NMR experiments provide improved sensitivity through ^{13}C detection, enhance resolution through additional frequency dimensions, enable measurements of orientation-dependent frequencies for all backbone and side chains sites, and provide mechanisms for making resonance assignments.

4. Experimental

4.1. Samples

The samples used to demonstrate the two- and three-dimensional triple-resonance experiments are single crystals of $^{13}C_{\alpha}$, ^{15}N labeled single crystal of N-acetyl leucine ($^{13}C_{\alpha}$,^{15}N NAL) and ^{15}N labeled N-acetyl valine (NAV); Pf1 coat protein in magnetically aligned phospholipid bilayers where the protein is labeled with $_{\alpha}$ and ^{15}N at all valine, leucine and isoleucine residues ($^{13}C_{\alpha}$, ^{15}N VLI Pf1); and Pf1 coat protein in magnetically aligned bacteriophage particles where the protein is labeled ~20% randomly with ^{3}C and ~100% uniformly with ^{15}N Pf1 (^{13}C, ^{15}N Pf1). The single crystal of $^{13}C_{\alpha}$, ^{15}N NAL was prepared by slow evaporation of aqueous solution after acetylating $^{13}C_{\alpha}$ and ^{15}N labeled leucine (Cambridge Isotope Laboratories, Andover, MA). Bacteriophage Pf1 was prepared as described previously [27]. Uniformly ~20% C and ~100% ^{15}N labeled bacteriophage was prepared using growth media obtained from Cambridge Isotope Laboratories, Inc. and selectively (Val, Leu, and Ile) $^{13}C_{\alpha}$ and ^{15}N labeled Pf1 was prepared using SLS media to avoid isotopic scrambling [31].

The sample of Pf1 coat protein in magnetically aligned bilayers was prepared as described previously [32,33]. The phospholipids were 1,2-dimyristoyl-sn-glycero-3-phospho-choline (DMPC) and 1,2-di-*O*-hexyl-sn-glycero-3-phospho-choline (6-O-PC) from Avanti Polar Lipids, Inc. (Alabaster, AL). Five milligrams of the lyophilized protein was dissolved in 200 μl of 100 mM 6-O-PC solution. The protein/6-O-PC solution was transferred to 43.4 mg of lyophilized DMPC. The resulting solution was vortexed and freeze-heated several times until it becomes a clear, nonviscous solution on ice. The molar ratio between long-chain lipids and short-chain lipids (q) was 3.2 and a lipid concentration was 26% (w/v). The pH of the sample was adjusted to 6.8 on ice. A flat-bottom NMR tube with a 5-mm outer diameter (New Era Enterprises, Vineland, NJ) was filled with 160 μl of the solution.

4.2. NMR instrumentation

The experimental spectra were obtained on a Varian Ino-va spectrometer with a Magnex 500/89 AS magnet using a homebuilt probe with a single 5 mm ID coil triple tuned to the ^{1}H, ^{13}C and ^{15}N resonance frequencies of 500.09, 125.76 and 50.68 MHz [18]. The ^{13}C and ^{15}N channels were isolated from each other using band-stop (parallel resonance) filters, which provide ~35 dB of isolation. This design is robust enough to withstand 25 ms of continuous irradiation on all three RF channels at power levels of 500, 200 and 100 W on the ^{15}N, ^{13}C and ^{1}H channels, respectively. For all the experiments, B_1 field strengths of 50 kHz were used unless otherwise indicated. ^{13}C chemical shifts are referenced by defining the high field peak of external adamantane to be 38.4 ppm and ^{15}N chemical shifts by defining the resonance of external ammonium sulphate to be 26.8 ppm [34].

Acknowledgments

We thank David Black for help with the preparation of the protein samples. This research was supported by grants RO1EB01966, RO1GM064676, and RO1GM066978 and utilized the Biomedical Technology Resource for NMR Molecular Imaging of Proteins, which is supported by P41EB002031.

References

1. Opella SJ, Marassi FM. Structure determination of membrane proteins by NMR spectroscopy. Chem. Rev. 2004; 104:3587–3606. [PubMed: 15303829]
2. Tien C, Gao PF, Pinto LH, Lamb RA, Cross TA. Initial structural and dynamic characterization of the M2 protein transmembrane and amphipathic helices in lipid bilayers. Protein Sci. 2003; 12:2597–2605. [PubMed: 14573870]

3. Kamihira M, Vosegaard T, Mason AJ, Straus SK, Nielsen NC, Watts A. Structural and orientational constraints of bacteriorho-dopsin in purple membranes determined by oriented sample solid-state NMR. J. Struct. Biol. 2005; 149:7–16. [PubMed: 15629653]
4. Cross TA, DiVerdi JA, Opella SJ. Strategy for nitrogen NMR analysis of biopolymers. J. Am. Chem. Soc. 1982; 104(6):1759–1761.
5. Waugh JS. Uncoupling of local field spectra in nuclear magnetic resonance-determination of atomic positions in solids. Proc. Natl. Acad. Sci. USA. 1976; 73:1394–1397. [PubMed: 1064013]
6. Cavanagh, J.; Fairbrother, WJ.; Palmer, AG.; Rance, M.; Skelton, NJ. Protein NMR Spectroscopy: Principles & Practice. second ed.. San Diego: Academic Press; 2006.
7. Castellani F, van Rossum B, Diehl A, Schubert M, Rehbein K, Oschkinat H. Structure of a protein determined by solid-state magic-angle-spinning NMR spectroscopy. Nature. 2002; 402:98–102. [PubMed: 12422222]
8. Heise H, Seidel K, Etzkorn M, Becker S, Baldus M. 3D NMR spectroscopy for resonance assignment and structure elucidation of proteins under MAS: Novel pulse schemes and sensitivity considerations. J. Magn. Reson. 2005; 173:64–74. [PubMed: 15705514]
9. Wand AJ, Bieber RJ, Urbauer JL, McEvog, Gan Z. Carbon relaxation in randomly fractionally ^{13}C-enriched proteins. J. Magn. Reson. B. 1995; 108:173–175. [PubMed: 7648015]
10. Kishore AI, Mayer MR, Prestegard JH. Partial ^{13}C isotope enrichment of nucleoside nomophosphatos: useful reporters for NMR structural studies. Nucl. Acid. Res. 2005; 33:e164.
11. De Angelis AA, Howell SC, Nevzorov A, Opella SJ. Structure determination of a membrane protein with two trans-membrane helices in aligned phospholipid bicelles by solid-state NMR spectros-copy. J. Am. Chem. Soc. 2006; 128:12256–12267. [PubMed: 16967977]
12. Hong M. Selective and extensive 13C labeling of a membrane protein for solid-state NMR investigation. J. Biomol. NMR. 1999; 14:71–74. [PubMed: 10382307]
13. Schneider DM, Tycko R, Opella SJ. High-resolution solid-state triple nuclear magnetic resonance measurement of carbon-13-nitro-gen-15 dipole–dipole couplings. J. Magn. Reson. 1987; 73(3): 568–573.
14. Ramanathan KV, Opella SJ. High-resolution solid-state carbon-13-nitrogen-14 and carbon-13-nitrogen-15 heteronuclear correlation spectroscopy. J. Magn. Reson. 1990; 86:227–235.
15. Gu ZT, Opella SJ. Two- and three-dimensional 1H/13C PISEMA experiments and their application to backbone and side chain sites of amino acids and peptides. J. Magn. Reson. 1999; 140:340–346. [PubMed: 10497041]
16. Gu Z, Opella SJ. Three-dimensional 13C shift/1H-15N coupling/ 15N shift solid-state NMR correlation spectroscopy. J. Magn. Reson. 1999; 138:193–198. [PubMed: 10341122]
17. Tan WM, Gu Z, Zeri AC, Opella SJ. Solid-state NMR triple-resonance backbone assignments in a protein. J. Biomol. NMR. 1999; 13:337–342. [PubMed: 10353195]
18. Sinha N, V Grant C, Rotondi KS, Feduik-Rotondi L, Gierasch LM, Opella SJ. Peptides and the development of double- and triple-resonance solid-state NMR of aligned samples. J. Pept. Res. 2005; 65:605–620. [PubMed: 15885119]
19. Fung BM, Khitriu AK, Ermolaev K. An improved broadband decoupling sequence for liquid crystals and solids. J. Magn. Res. 2000; 142:97–101.
20. Neeraj, Sinha; Grant, CV.; De Angelis, AA.; Howell, SC.; Opella, SJ. SPINAL modulated decoupling in high field double- and triple-resonance solid-state NMR experiments on stationary samples. J. Magn. Res. 2005; 177:197–202.
21. Ishii Y, Tycko R. Multidimensional heteronuclear correlation spectroscopy of a uniformly ^{15}N- and ^{13}C-labeled peptide crystal: Toward spectral resolution assignment and structure determination of oriented molecules in solid-state NMR. J. Am. Chem. Soc. 2000; 122:1443–1455.
22. Vosegaard T, Nielsen NC. Towards high-resolution solid-state NMR on large uniformly ^{15}N- and [^{13}C,^{15}N]-labeled membrane proteins in oriented lipid bilayers. J. Biomol. NMR. 2002; 22:225–247. [PubMed: 11991353]
23. Pines A, Gibby MG, Waugh JS. Proton-enhanced nuclear induction spectroscopy. A method for high resolution NMR of dilute spins in solids. J. Chem. Phys. 1972; 56:1776–1777.

24. Schaefer J, McKay RA, Stejskal EO. Double-cross-polarization NMR of solids. J. Magn. Res. 1979; 34:443–447.
25. Wu CH, Ramamoorthy A, Opella SJ. High resolution heteronu-clear dipolar solid-state NMR spectroscopy. J. Magn. Reson. A. 1994; 109:270–272.
26. Gan Z. Spin dynamics of polarization spin exchange at the magic angle in multiple spin systems. J. Magn. Reson. 2000; 143:136–143. [PubMed: 10698654]
27. Thiriot DS, Nevzorov AA, Zagyanskiy L, Wu CH, Opella SJ. Structure of the coat protein in Pf1 bacteriophage determined by solid-state NMR spectroscopy. J. Mol. Biol. 2004; 341:869–879. [PubMed: 15288792]
28. Cross TA, Frey MH, Opella SJ. Nitrogen-15 spin exchange in a protein. J. Am. Chem. Soc. 1983; 105:7471–7473.
29. Gullion T, Baker DB, Conradi MS. New compensated Carr- Purcell sequence. J. Magn. Reson. 1990; 89:479–484.
30. States DJ, Haberkorn RA, Rubin DJ. A two-dimensional nuclear overhauser experiment with pure absorption in four quadrants. J. Magn. Res. 1982; 48:286–292.
31. Park SH, De Angelis AA, Nevzorov A, Wu CH, Opella SJ. Three-dimensional structure of the transmembrane domain of Vpu from HIV-1 in aligned phospholipid bicelles. Biophys. J. 2006; 91:3032–3042. [PubMed: 16861273]
32. Giesen AW, Bae LC, Barrett CL, Chyba JA, Chaykovsky MM, Cheng MC, Murray JH, Oliver EJ, Sullivan SM, Dahlquist FW, Homans SW, Brown JM. Measurement of one-bond $^{1}H_{\alpha}$– $^{13}C_{\alpha}$ couplings in backbone-labelled proteins. J. Biomed. NMR. 2001; 19:255–260.
33. De Angelis AA, Nevzorov AA, Park SH, Howell SC, Mrse AA, Opella SJ. High-resolution NMR spectroscopy of membrane proteins in aligned bicelles. J. Am. Chem. Soc. 2004; 127:15340–15341. [PubMed: 15563135]
34. Morcombe CR, Zilm KW. Chemical shift referencing in MAS solid state NMR. J. Magn. Res. 2003; 162:479–486.

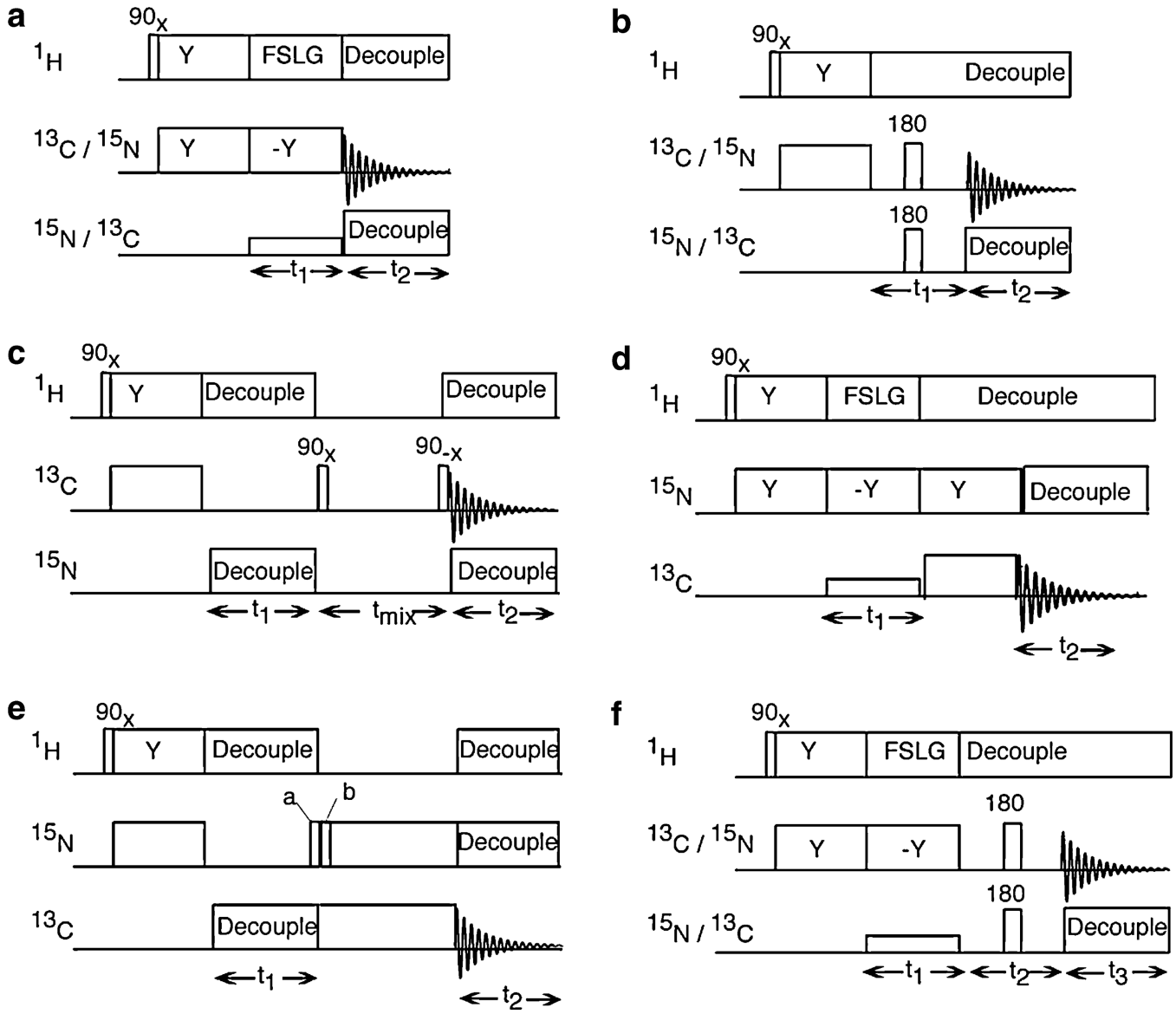

Fig. 1.

Timing diagrams for triple-resonance solid-state NMR experiments. (a) Two-dimensional ^{1}H–^{13}C or ^{1}H–^{15}N PISEMA. The pulse sequence for the triple resonance version of the PISEMA is same as its double resonance version except that low power irradiation (mismatched to the irradiations in the other two channels) is applied during t_1 period at the resonance frequency of the undetected nucleus. (b) Two-dimensional ^{13}C–^{15}N dipolar coupling measurement. The phase of the 180° pulse is same as for the cross-polarization irradiation. The receiver phase is cycled as (x, —x) and the 90° pulse on the ^{1}H channel is phase cycled as (x, −x). (c) Twoα-dimensional ^{13}C/^{13}C spin exchange. The 90° pulse after the t_1 period is phase incremented by 90° for quadrature detection. (d) Two-dimensional ^{1}H–^{15}N PISEMA with ^{13}C detection. (e) Two-dimensional ^{13}C/^{15}N HETCOR. (f) Three-dimensional ^{1}H–^{13}C dipolar coupling/^{13}C–^{15}N dipolar coupling/^{13}C chemical shift or ^{1}H–^{15}N coupling/^{13}C–^{15}N dipolar coupling/^{15}N chemical shift correlation.

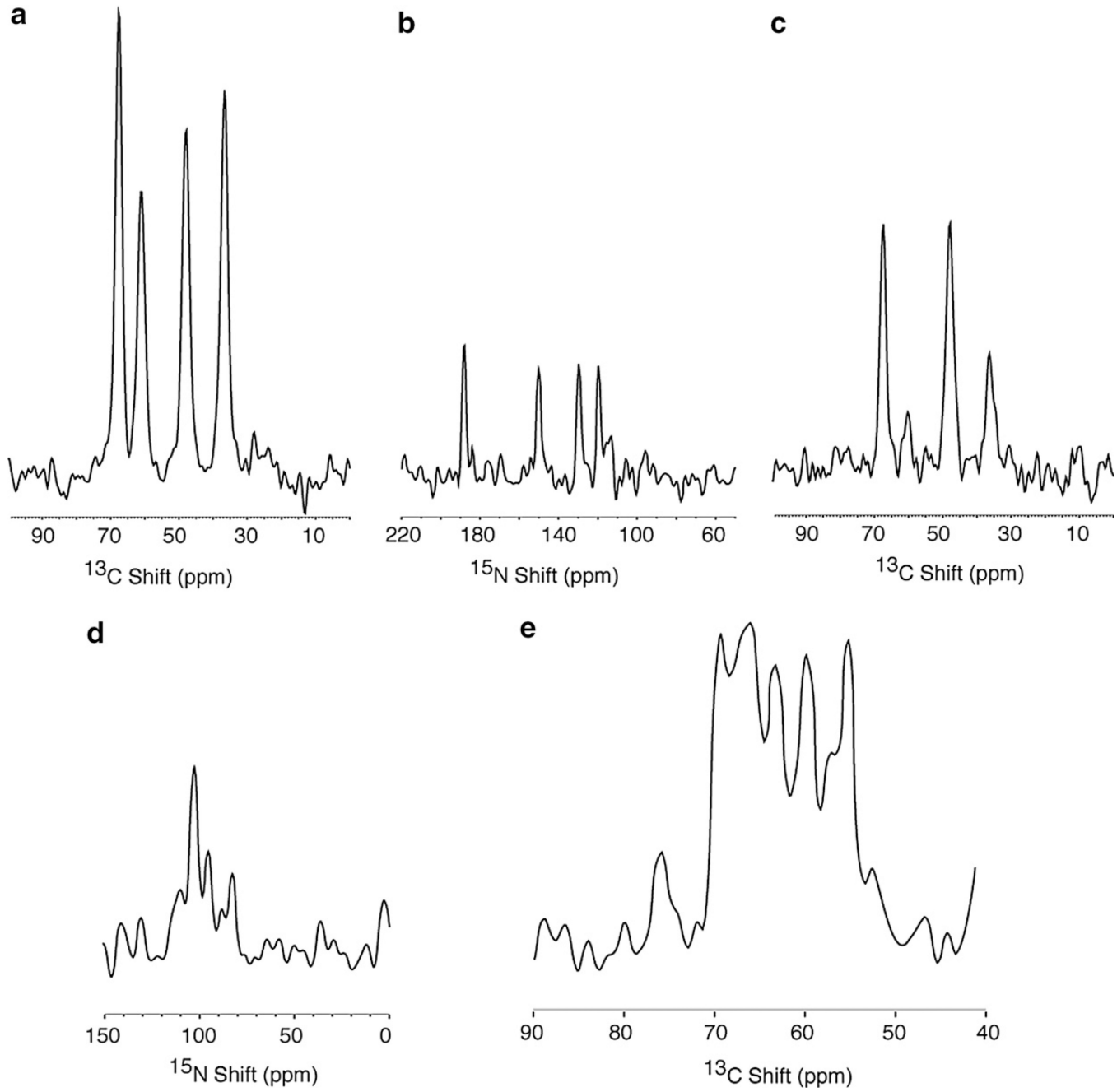

Fig. 2.

Comparison of ^{13}C and ^{15}N detected one-dimensional NMR spectra. (a–c) are from the $^{13}C_{\alpha}$, ^{15}N labeled single crystal of *N*-acetyl leucine ($^{13}C_{\alpha}$, ^{15}N NAL), and resulted from signal averaging 8 scans. The four resonances in the spectrum correspond to the four molecules in the unit cell of the crystal. (d) and (e) are from the Pf1 coat protein in magnetically aligned phospholipid bilayers where the protein is labeled with $^{13}C_{\alpha}$ and ^{15}N at all valine, leucine and isoleucine residues ($^{13}C_{\alpha}$, ^{15}N VLI Pf1), and resulted from signal averaging 256 scans. The ^{1}H and ^{15}N (or ^{13}C) decoupling fields applied during data acquisition were 50 kHz. All of the cross-polarization mix times were 1 msec and the recycle delays 6 s. (a) ^{13}C detection following cross-polarization. (b) ^{15}N detection

following cross-polarization. (c) ^{13}C detection following double-cross-polarization. (d) ^{15}N detection following cross-polarization. (e) ^{13}C detection following cross-polarization.

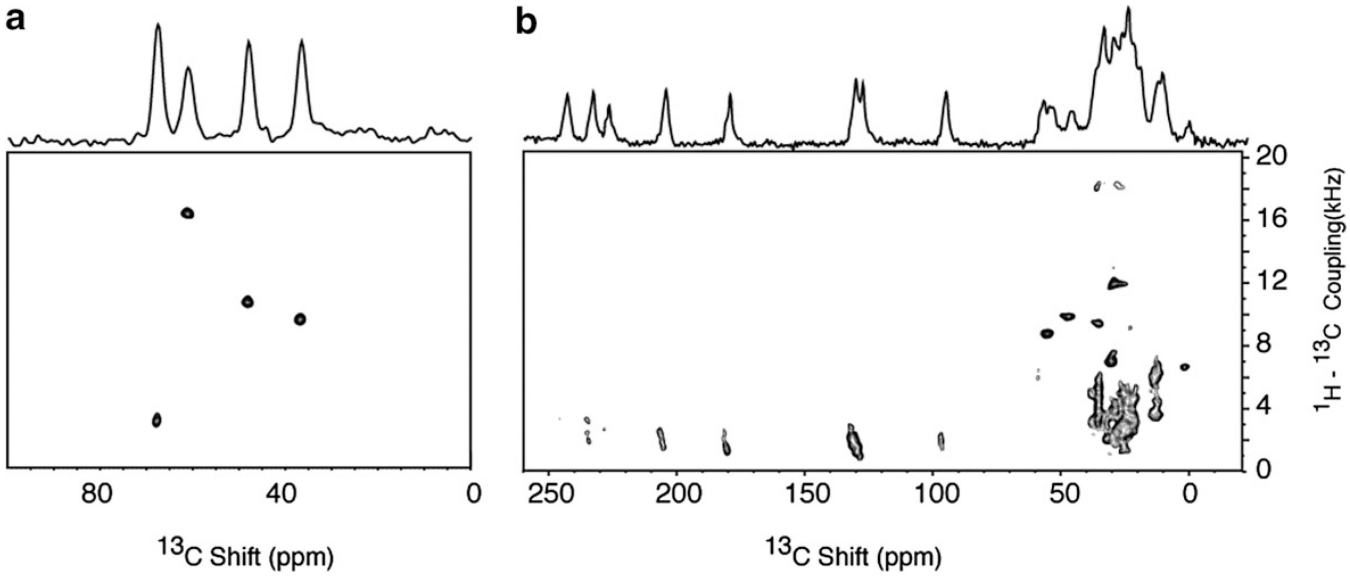

Fig. 3.

Two-dimensional ^{1}H–^{13}C PISEMA spectra obtained using the pulse sequence in Fig. 1a. (a) Spectrum from the $^{13}C_{\alpha}$, ^{15}N labeled single crystal of *N*-acetyl leucine ($^{13}C_{\alpha}$, ^{15}N NAL) obtained with 4 scans for each of 128 t1 points. (b) Spectrum from the ^{15}N labeled single crystal of *N*-acetyl valine (NAV) obtained with 8 scans for each of 128 t1 points. During the heteronuclear spin exchange period (t1), the radiofrequency field strength of 55 kHz power level on the ^{1}H channel enabled the maximum ^{1}H–^{13}C dipolar couplings to be observed without aliasing. The recycle delay was 6 s. The two-dimensional data sets were zero filled to 1K data points and multiplied by a sine bell window function in both dimensions before double Fourier transformation.

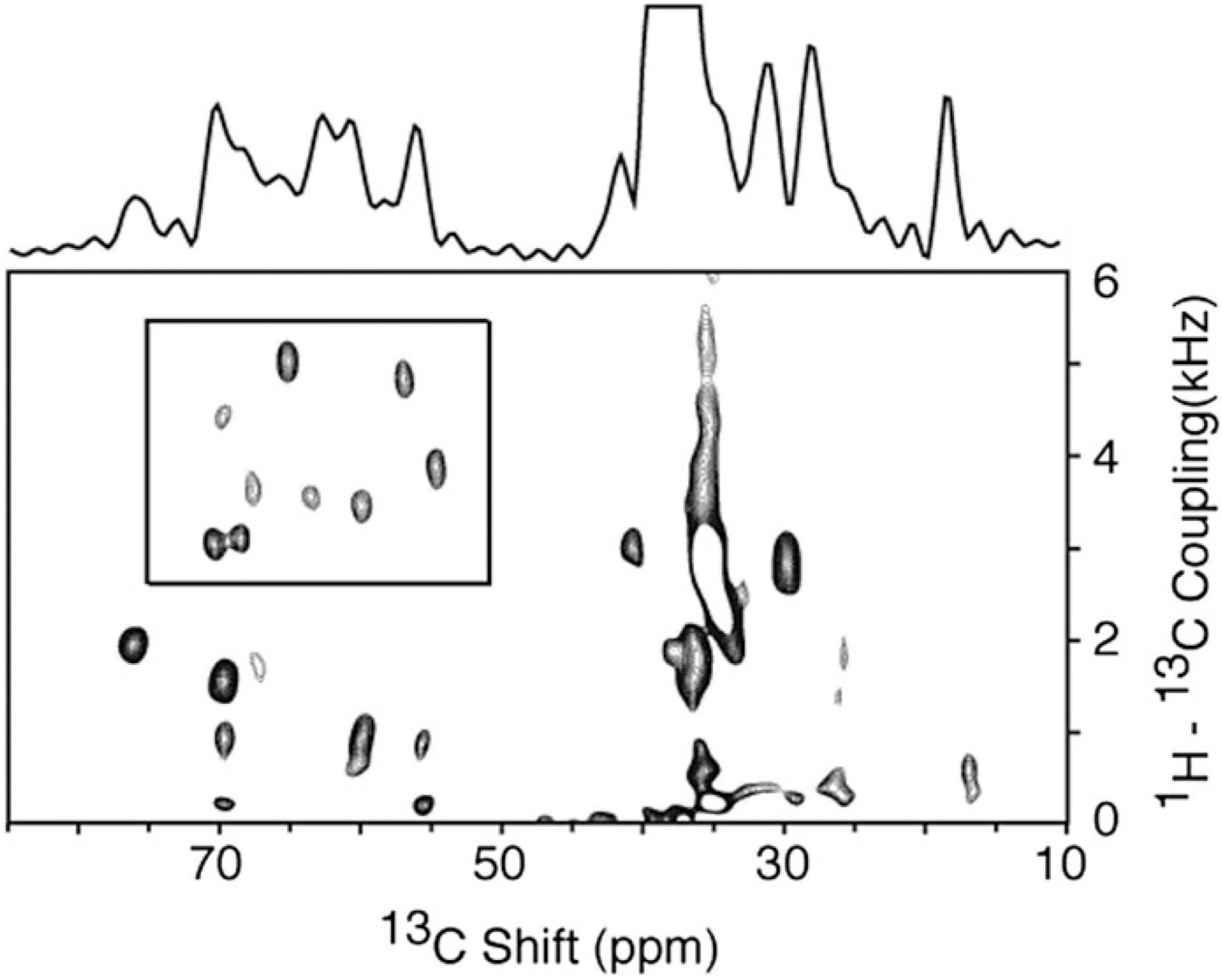

Fig. 4.

Two-dimensional ^{1}H–^{13} C PISEMA spectrum of the membrane-bound form of the 46-residue Pf1 coat protein in magnetically aligned phospholipid bilayers where the protein is labeled with $^{13}C_{\alpha}$ and N at all valine, leucine and isoleucine residues ($^{13}C_{\alpha}$, N VLI Pf1). The spectrum was obtained using the pulse sequence in Fig. 1a. All of the signals in the box are from ^{1}H–$^{13}C_{\alpha}$ dipolar couplings. Nearly all of the other intensity observed in the spectrum in from the natural abundance signals from the phospholipids in the sample. Ninety six scans were acquired for each of 128 points in the indirect dimension. The recycle delay was 5 s and the temperature 40 °C. The two-dimensional data set was zero filled to 1K data points and multiplied by a sine bell window function in both dimensions before double Fourier transformation.

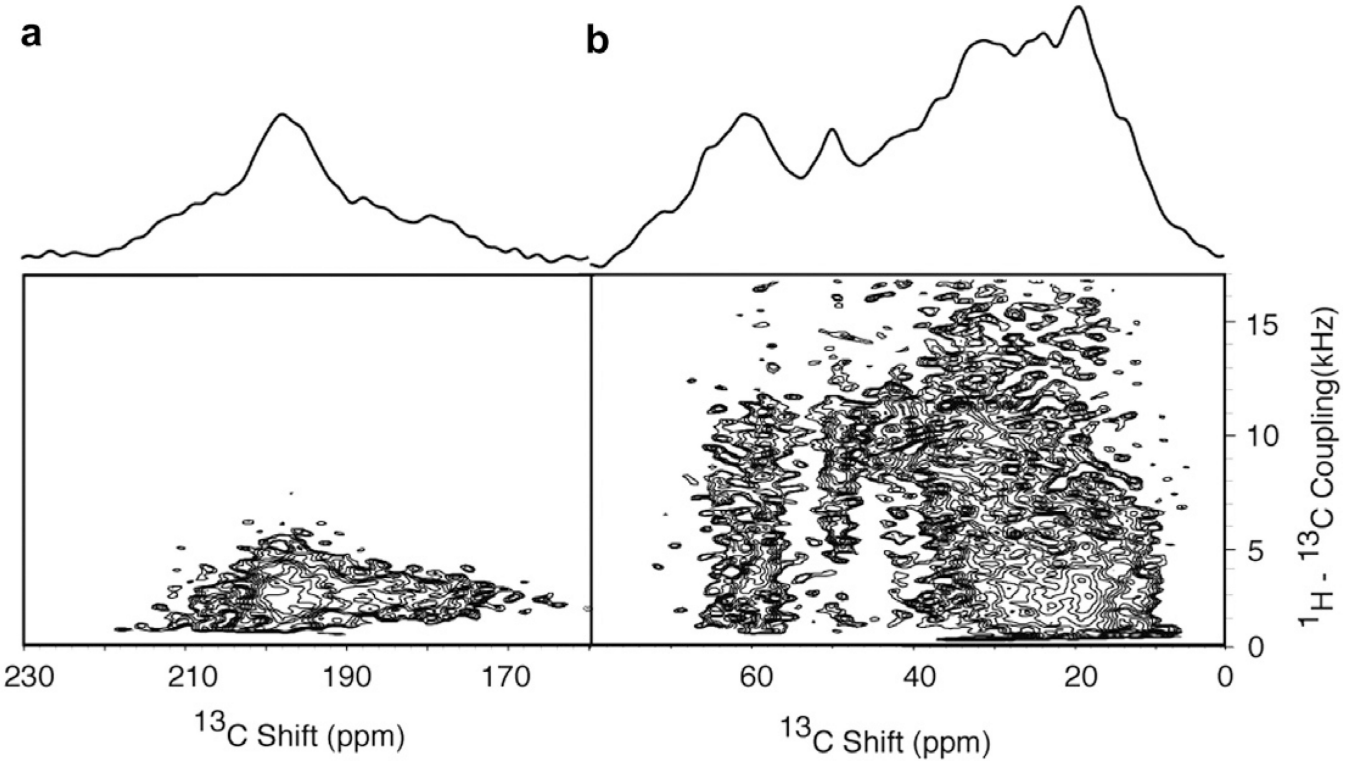

Fig. 5.

Two-dimensional ^{1}H–^{13} C PISEMA spectrum of the structural form of the 46-residue Pf1 coat protein in magnetically aligned virus particles where the protein is labeled ~20% randomly with ^{3}C and ~100% uniformly with ^{15}N Pf1 (^{13}C and ^{15}N Pf1). (a) Carbonyl and carboxyl carbon resonances. (b) Aliphatic carbon resonances. Thirty two scans were acquired for each of 128 points in the indirect dimension. The recycle delay was 6 s, and the temperature 0 °C. The central ^{1}H carrier frequency during t_1 was +2 ppm relative to the water resonance during the PISEMA portion of the pulse sequence. The two-dimensional data set was zero filled to 1K data points and multiplied by a sine bell window function in both dimensions before double Fourier transformation.

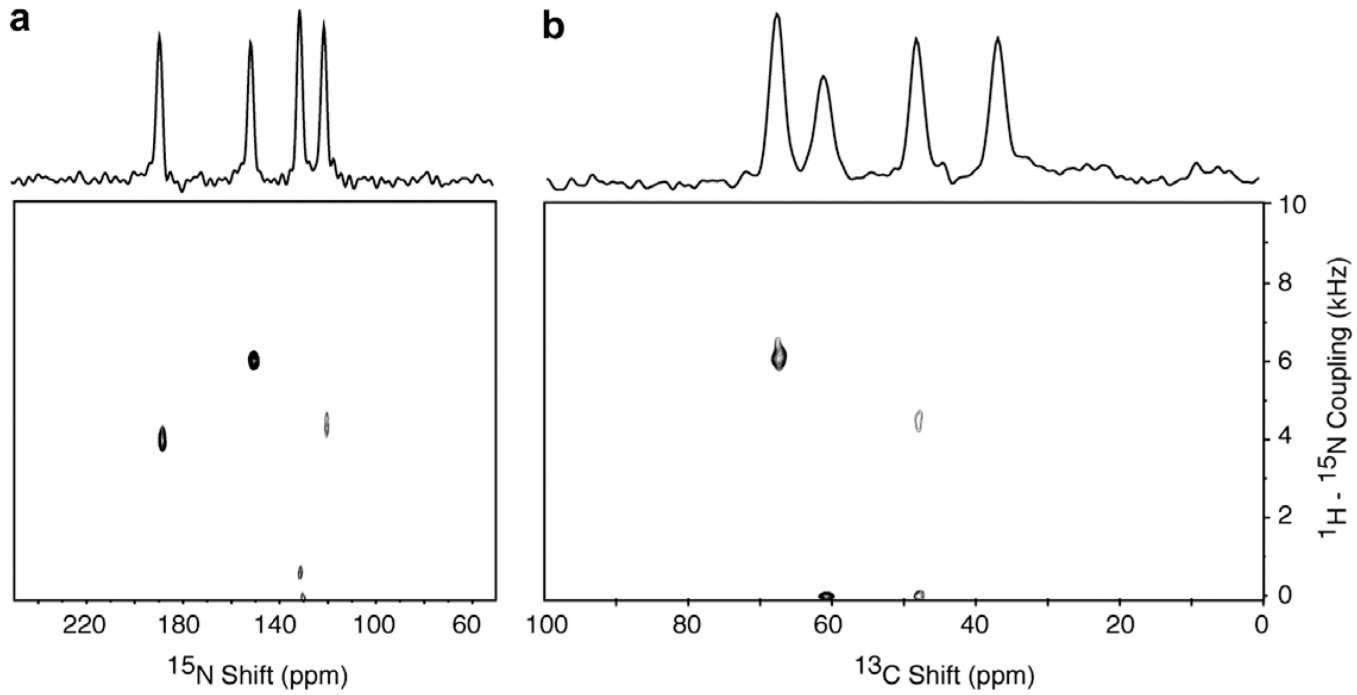

Fig. 6.

Two-dimensional ^{1}H–^{15}N PISEMA spectra of the $^{13}C_{\alpha}$, ^{15}N labeled single crystal of *N*-acetyl leucine ($^{13}C_{\alpha}$, ^{15}N NAL). (a) ^{15}N detected. (b) ^{13}C detected. Sixteen scans were acquired for each of 128 points in the indirect dimension for spectrum a and 32 scans for spectrum b. The contact time was 1.0 ms during the double cross-polarization from ^{15}N to ^{13}C, and the recycle delay was 5 s.

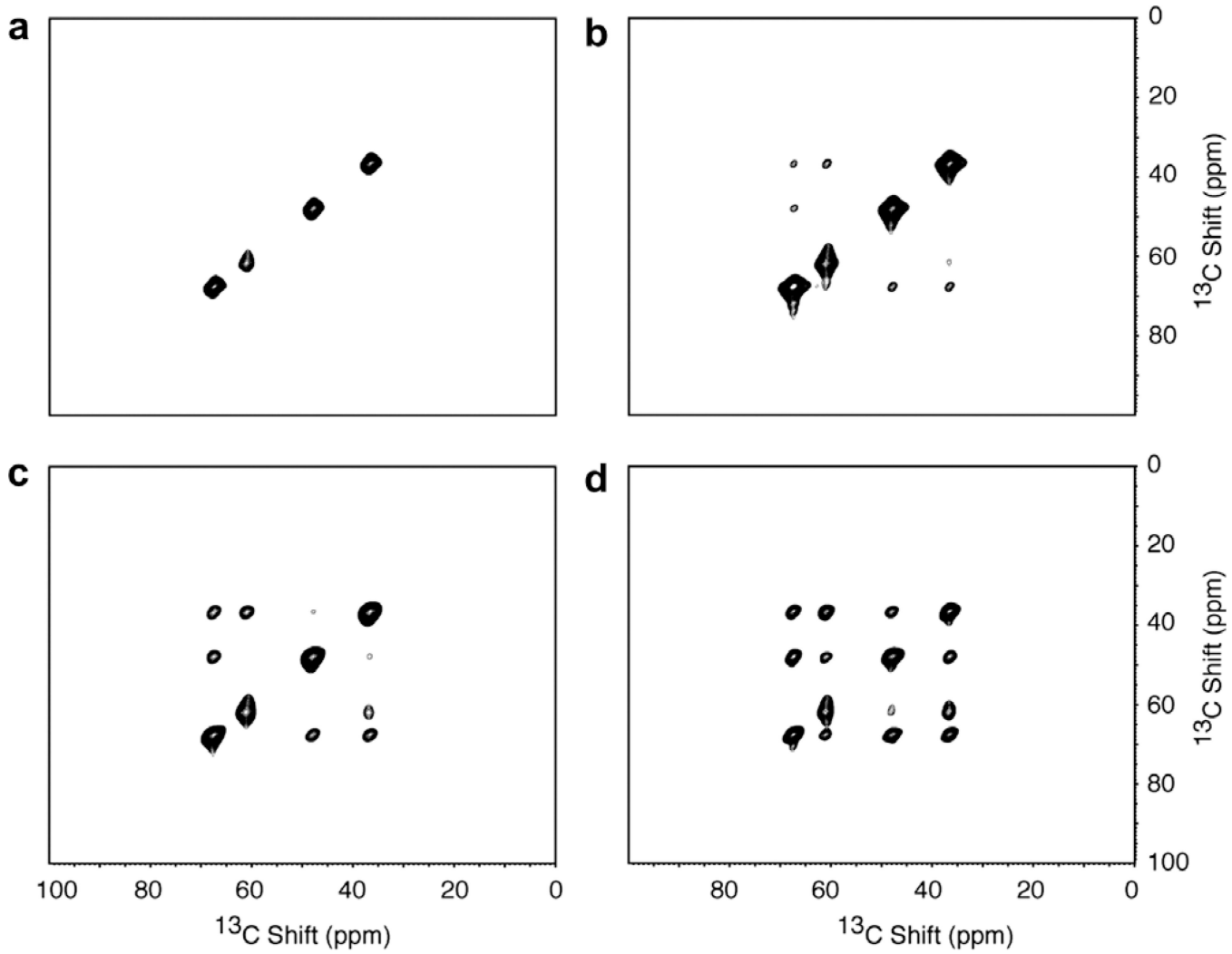

Fig. 7.

Two-dimensional homonuclear $^{13}C/^{13}C$ spin-exchange spectra obtained from the $^{13}C_{\alpha}$, ^{15}N labeled single crystal of *N*-acetyl leucine ($^{13}C_{\alpha}$, ^{15}N NAL) at various mix times in the pulse sequence in Fig. 1c. (a) 0.5 s. (b) 1.0 s. (c) 2.0 s. (d) 4.5 s. Eight scans for 90 t1 points were acquired with a 50 μs dwell for each spectrum. The ^{1}H and ^{15}N decoupling fields applied during the experiment were 50 kHz.

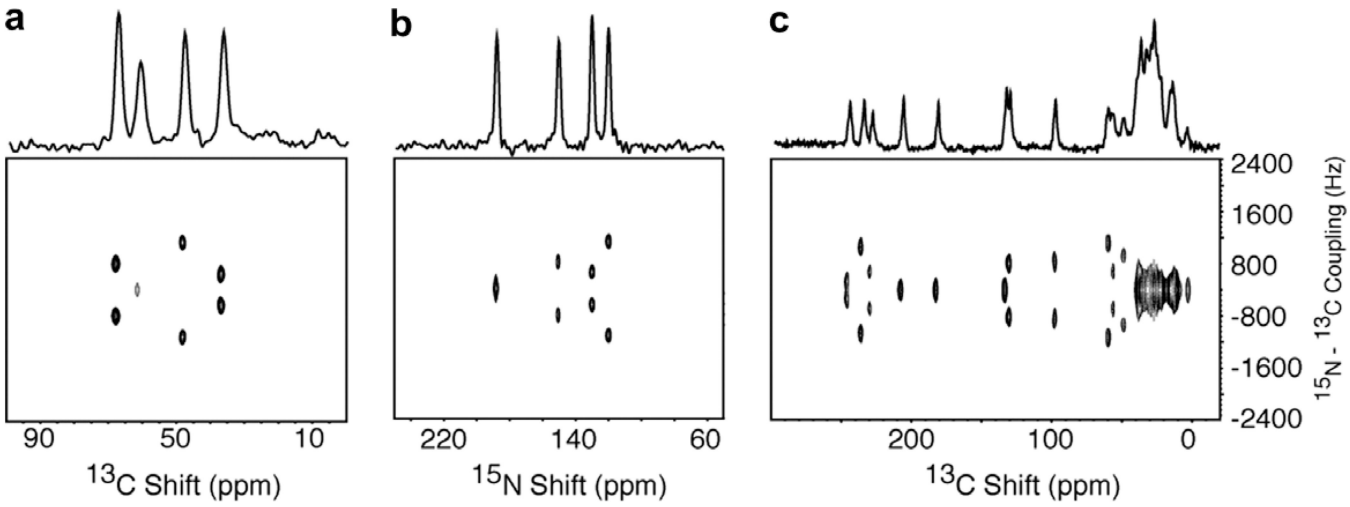

Fig. 8.

Two-dimensional ^{13}C–^{15}N SLF spectra obtained using the pulse sequence in various mix times in the pulse sequenceFig. 1b. (a) and (b) are from the $^{13}C_{\alpha}$, ^{15}N labeled single crystal of *N*-acetyl leucine ($^{13}C_{\alpha}$, ^{15}N NAL). (c) Is from the ^{15}N labeled single crystal of *N*-acetyl valine (NAV). (a) and (c) ^{13}C detected. (b) ^{15}N detected. For spectra a and b, four scans were collected for 48 points in the indirect dimension with 100 μs dwell time and 16 scans were collected for spectrum c.

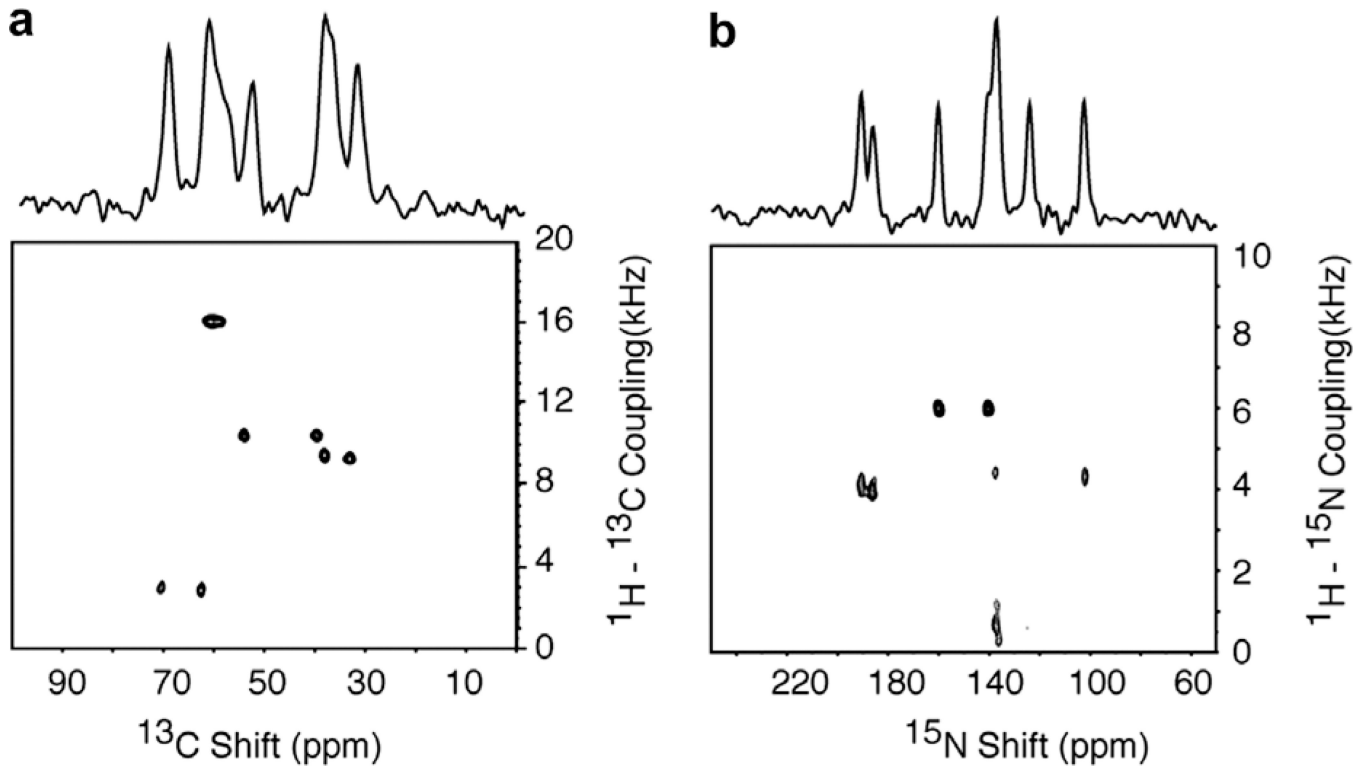

Fig. 9.

Two-dimensional PISEMA spectra of the $^{13}C_{\alpha}$, ^{15}N labeled single crystal of N-acetyl leucine ($^{13}C_{\alpha}$, ^{15}N NAL). (a) ^{1}H–^{13}C PISEMA spectrum obtained without ^{15}N decoupling during acquisition (t_2). (b) ^{1}H–^{15}N PISEMA spectrum obtained without ^{13}C decoupling during acquisition (t_2). For the 2D spectrums, 4 scans were added for each t_1 points (128). During spin exchange period, 55 kHz power level on the ^{1}H channel were used. The two-dimensional data sets were zero filled to 1K data points and multiplied by sine bell window function before double Fourier transformation. The one-dimensional ^{13}C (a) and ^{15}N (b) NMR spectra obtained without decoupling of the unobserved nucleus are aligned along the corresponding two-dimensional spectra.

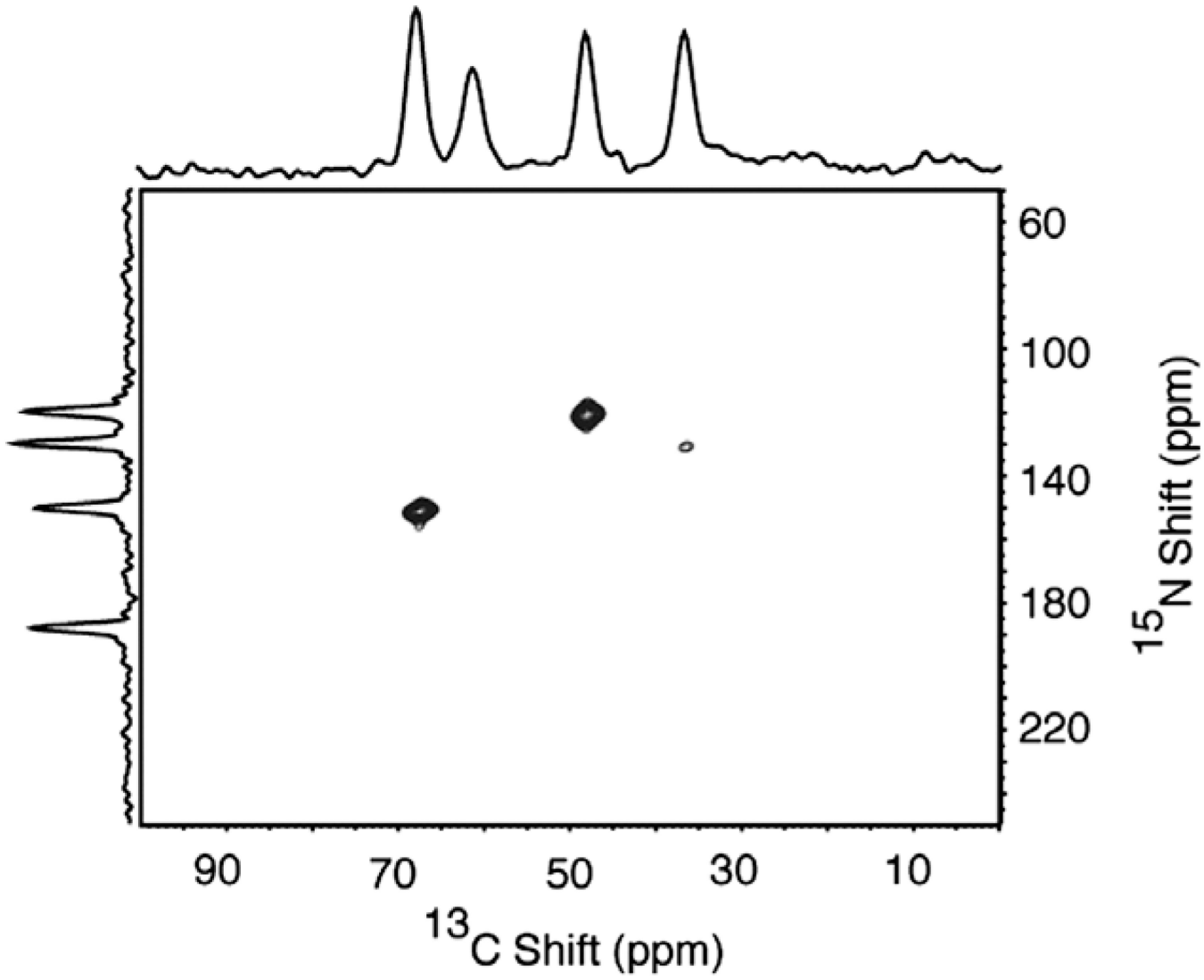

Fig. 10.

Two-dimensional $^{15}N/^{13}C$ HETCOR spectrum of the $^{13}C_{\alpha}$, ^{15}N labeled single crystal of N-acetyl leucine ($^{13}C_{\alpha}$, ^{15}N NAL) obtained using the pulse sequence in Fig. 1e. Four scans for each of 90 t_1 points were acquired in the indirect dimension with a dwell of 50 μs. The ^{1}H decoupling field during the t_1 and t_2 intervals was 50 kHz. The recycle delay used for the experiment was 6 s.

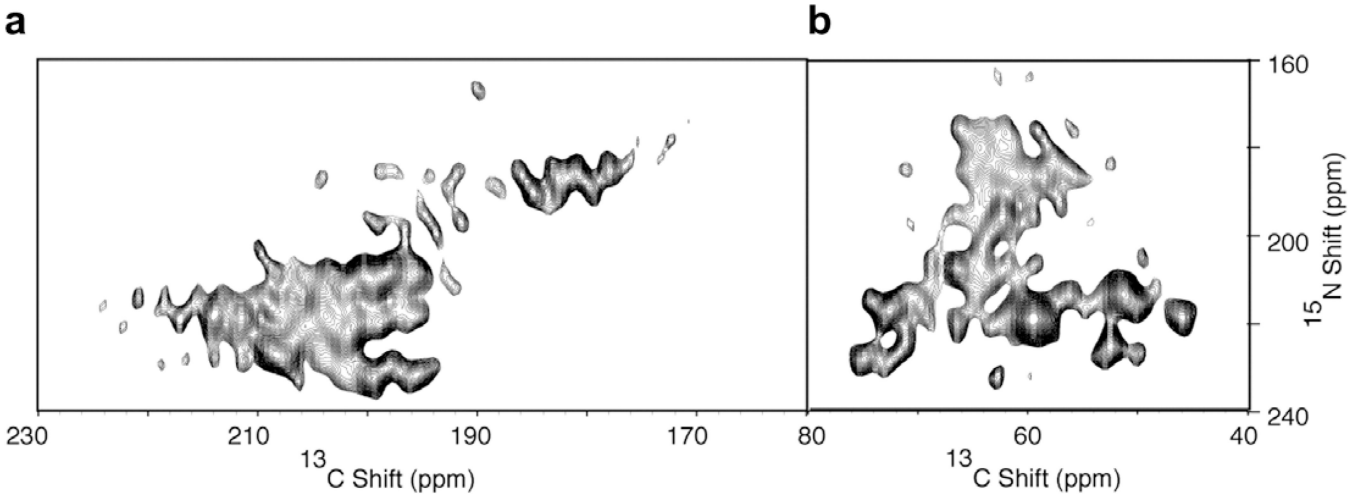

Fig. 11.

Two-dimensional $^{15}N/^{13}C$ HETCOR spectrum of the magnetically aligned sample of Pf1 bacteriophage with the coat protein labeled with both ^{13}C and ^{15}N. The spectrum was acquired at 0 °C. Thirty two scans of 80 complex points were acquired in the indirect dimension with a spectral width of 30 kHz. The recycle delay was 6 s. The data were zero filled to 1K points and multiplied by a sine bell window function in both dimensions prior to double Fourier transformation. The carrier frequency for ^{13}C irradiation was in the center of the spectrum, between the aliphatic and carbonyl resonance regions, and the double cross-polarization was optimized for both types of resonances.

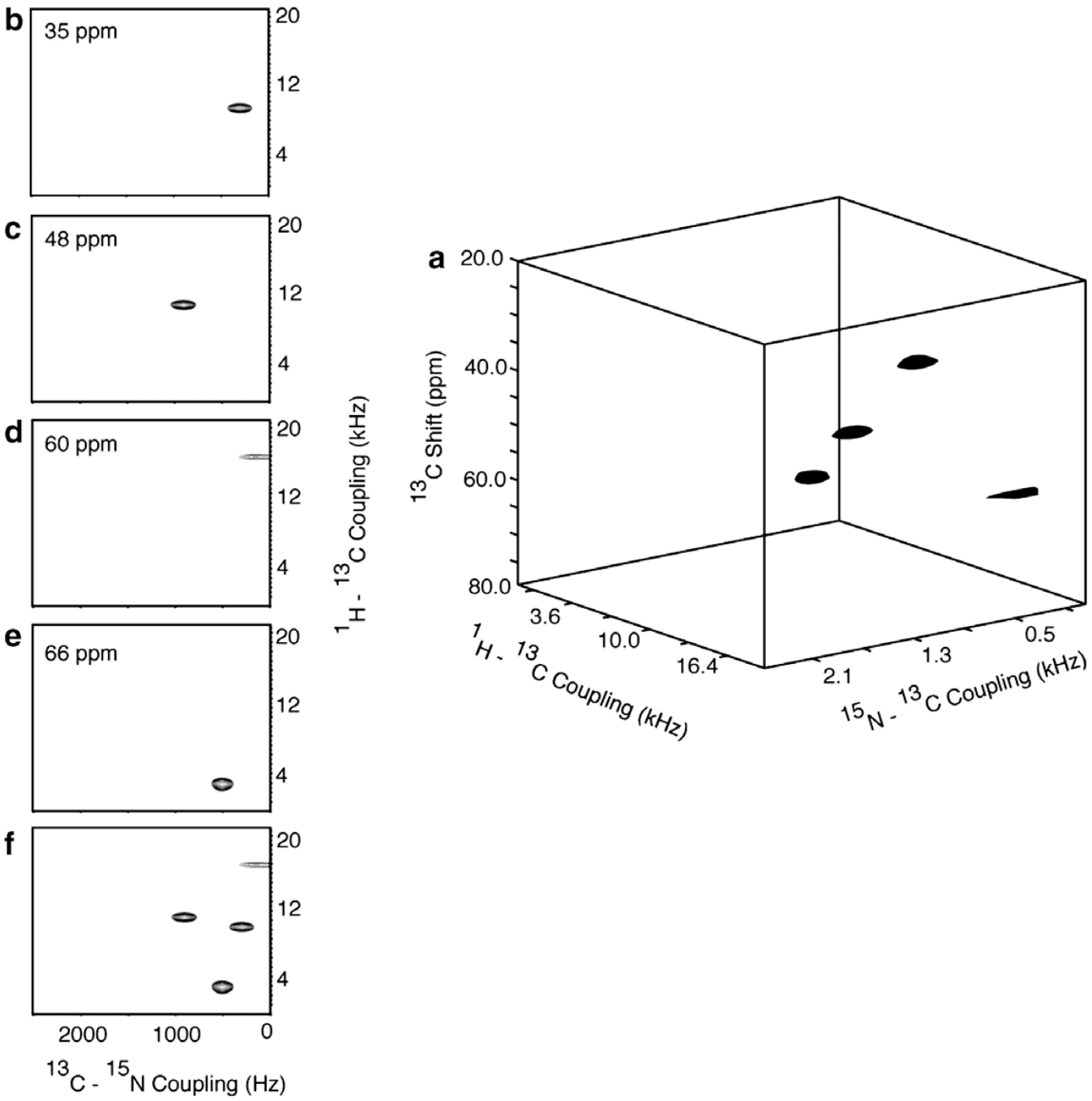

Fig. 12.

Results from the three-dimensional experiment diagrammed in Fig. 1f that correlates ^{13}C chemical shift/^{1}H–^{13}C dipolar coupling/^{13}C–^{15}N dipolar coupling frequencies performed on the $^{13}C_{\alpha}$, ^{15}N labeled single crystal of *N*-acetyl leucine ($^{13}C_{\alpha}$, ^{15}N NAL). (a) Three-dimensional cube displaying all four resonances. (b)–(e) Two-dimensional planes at ^{13}C chemical shift frequencies containing resonance intensity. (f) Two-dimensional projection. 32 points in the ^{1}H–^{13}C dimensions (spectral width = 40 kHz) and 21 points in the ^{13}C–^{15}N dimensions (spectral width = 5.0 kHz) were acquired with 4 scans.

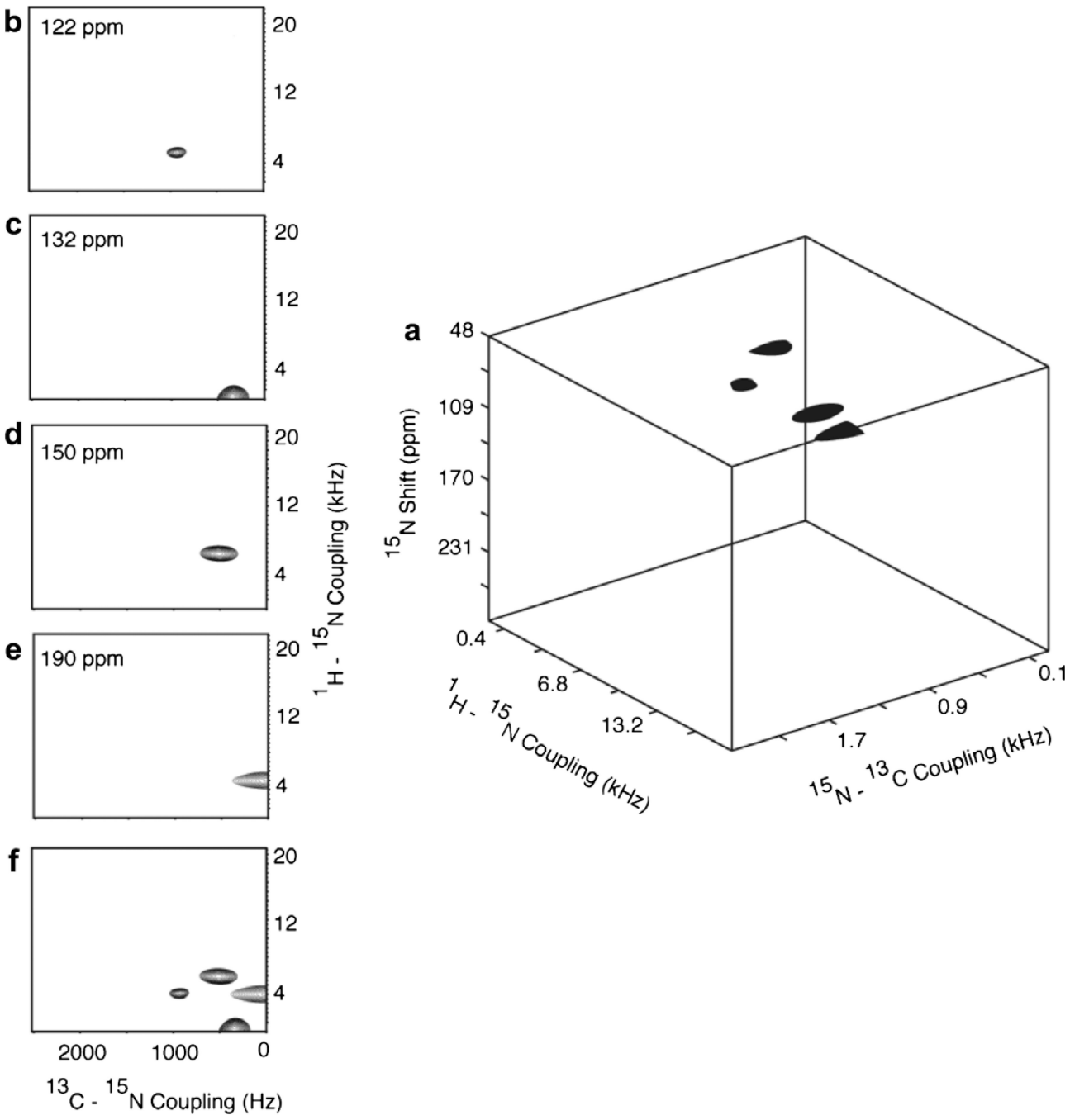

Fig. 13.

Results from the three-dimensional experiment diagrammed in Fig. 1f that correlates ^{15}N chemical shift/^{1}H–^{15}N dipolar coupling/^{13}C–^{15}N dipolar coupling frequencies performed on the $^{13}C_{\alpha}$, ^{15}N labeled single crystal of *N*-acetyl leucine ($^{13}C_{\alpha}$, ^{15}N NAL). (a) Three-dimensional cube displaying all four resonances. (b)–(e) Two-dimensional planes at ^{15}N chemical shift frequencies containing resonance intensity. (f) Two-dimensional projection. 32 points in the ^{1}H–^{15}N dimensions (spectral width = 40 kHz) and 21 points in the ^{13}C–^{15}N dimensions (spectral width = 5.0 kHz) were acquired with 4 scans.